Isovector giant quadrupole resonance in the $^{40}Ca(n,\gamma_0)$ reaction

C. M. Laymon, R. O. Nelson, and S. A. Wender
Los Alamos National Laboratory, Los Alamos, New Mexico 87545

L. R. Nilsson
The Svedberg Laboratory, Uppsala, Sweden
(Received 7 July 1992)

The fore-aft asymmetry and the 90° differential cross section in the $^{40}Ca(n,\gamma_0)$ reaction were measured from $E_n = 8$ to 44 MeV. An energy-dependent asymmetry is observed that is interpreted as the result of the isovector giant quadrupole resonance interfering with background $E1$ amplitudes. The present data agree with previous low-energy data. At higher incident neutron energies, the present data do not agree with the predictions of a direct-semidirect model calculation based on the low-energy data alone. Calculations using the pure resonance model are in agreement with the data.

PACS number(s): 25.40.Lw, 21.10.Re, 27.40.+z

I. INTRODUCTION

Giant resonances in nuclei have been under experimental and theoretical investigation for many years [1–3]. In some areas our knowledge is extensive. For example, the systematics of the isovector giant dipole resonance (GDR) built on the ground state are well understood, and significant progress has been made in the study of excited state GDR's [3,4]. Much of the success in our understanding of the GDR is a consequence of its strong excitation by electromagnetic probes. Photoabsorption and radiative capture experiments have been particularly fruitful because of their selectivity. There are other elementary modes of excitation of both isoscalar and isovector nature that are predicted by collective models of the nucleus, such as the hydrodynamic models [3], which were first used to describe the GDR. These other modes have proven to be more difficult to study than the GDR because of the lack of selective probes and it has been necessary to use a variety of techniques.

Discussions of isovector giant quadrupole resonance (IVGQR) studies can be found in review articles [1–3]. Much of our knowledge on the subject has come from inelastic electron scattering [5] which tends to excite many multipoles. The complicated spectra from these experiments were interpreted as providing evidence for the IVGQR.

Radiative capture and photonuclear reactions have been another productive class of experiments in the study of the IVGQR. Much of the early work involved protons in the initial or final states. For example, Stewart and co-workers [6] measured the angular distribution of protons from the $^{16}O(\gamma,p)^{15}N$ reaction and interpreted their results as indicating the presence of quadrupole strength above the peak of the GDR. Snover *et al.* [7] used the reaction $^{208}Pb\ (p,\gamma)^{209}Bi$, in which capture to the ground and first two excited states of ^{209}Bi were not resolved, and identified a quadrupole resonance above the GDR in the presence of a direct $E2$ background. Recently, Feldman *et al.* [8] examined the γ_0 and γ_1 yield from polarized proton capture on ^{30}Si and interpreted the differential cross sections and analyzing powers as evidence for an IVGQR built on the first excited state of ^{31}P. They also concluded that the γ_0 results did not require a ground-state IVGQR since all the deduced $E2$ strength could be accounted for by direct capture.

Capture and photonuclear reactions involving neutrons are particularly effective ways of studying the IVGQR because the interpretation of these experiments is simpler than those involving protons. In neutron capture reactions, the direct process in which the neutron is captured into the final ground state with the simultaneous emission of a photon and without the excitation of the intermediate giant resonance can take place only via nuclear recoil. In this case the direct amplitude is multiplied by the kinematic effective charge. For quadrupole capture, this suppresses the direct $E2$ amplitude by a factor of $Z/[(A-1)^2+Z-1]$ [9] or 1.2% for ^{41}Ca relative to direct proton capture.

Because the amplitude for exciting the IVGQR in radiative capture and photonuclear reactions is small compared to $E1$ amplitudes, observation of the IVGQR in cross-section measurements is difficult, and one can achieve better sensitivity by exploiting interference effects. For example, in the measurement of a radiative capture cross section, the IVGQR would appear as a distortion in the high energy tail of the GDR and direct $E1$ capture cross section and would be difficult or impossible to extract. The fore-aft asymmetry defined as

$$A(\theta)=[Y(\theta)-Y(\pi-\theta)]/[Y(\theta)+Y(\pi-\theta)]$$

is a measure of interference between opposite parity amplitudes; as such, it is sensitive to a resonating $E2$ amplitude in the presence of an $E1$ background.

Drake *et al.* [10] measured the fore-aft asymmetry in the $^{208}Pb(n,\gamma)^{209}Pb$ capture reaction, and found a rise in the asymmetry that they attributed to $E1$-$E2$ interference at the expected position of the IVGQR. Berqvist *et al.* [11] used a similar technique to examine the giant resonance region in ^{41}Ca and also saw a rise in the asymmetry

that they attributed to interference between the IVGQR and $E1$ amplitudes from direct and resonant capture. The results were interpreted within the framework of the direct-semidirect (DSD) model. Both of these capture experiments were performed using tandem Van de Graaf accelerators and were therefore limited in the energy range that could be covered. In the case of Ref. [11] the maximum neutron energy of the experiment was 28 MeV.

The inverse reaction (γ,n) has also been employed to study the IVGQR. Phillips and Johnson [12] interpreted their results from the $^{16}O(\gamma,n)^{15}O$ reaction as an indication of a concentration of quadrupole strength above the GDR. Recently Murakami *et al.* [13–15] reported energy-dependent asymmetries in (γ,n) reactions on ^{40}Ca, ^{nat}Pb, and ^{nat}Cd.

Experiments at the Los Alamos Meson Physics Facility (LAMPF) [16,17] using the charge exchange reactions $(\pi^{\pm},\pi^{0})$ on nuclei ranging from ^{40}Ca to ^{208}Pb have established the existence of a substantial concentration of isovector monopole strength in agreement with distorted-wave-impulse-approximation–random-phase-approximation (DWIA-RPA) calculations of Auerbach and Klein [18]. Interestingly, these experiments revealed no evidence of the IVGQR also predicted by the calculations. This led the authors to speculate that the (e,e') experiments [5] had been misinterpreted. They suggested that much of the structure identified as isovector $E2$ strength was in fact a manifestation of the isovector giant monopole resonance (IVGMR) which occurs at approximately the same excitation energy. Tabor *et al.* [19] used the charge exchange reaction ^{40}Ca $(^{3}He,t)$ and also failed to find evidence for the IVGQR.

In the experiment reported here we have used a spallation neutron source to measure the differential cross section for the $^{40}Ca(n,\gamma_0)^{41}Ca$ at laboratory angles of 55°, 125°, and 90°. An advantage of using this reaction is that it has a high Q-value of 8.36 MeV so that there is little background under the ground-state capture peak from other gamma-producing processes or from neutrons scattered into the detector. Additionally the ground and first excited states of ^{41}Ca are separated by 1.94 MeV allowing separation of the γ-ray yield to the ground state. The goal of the experiment was to extend the work of Ref. [11] to higher energies in order to better investigate the IVGQR in ^{41}Ca.

II. EXPERIMENTAL PROCEDURE

The $^{40}Ca(n,\gamma_0)^{41}Ca$ experiment was performed at the Weapons Neutron Research (WNR) spallation neutron source target area at LAMPF. The neutron source has been described in previous publications [20,21] and only the basic features are reviewed here. Neutrons are produced in spallation reactions, induced by the 800-MeV LAMPF proton beam, in a 3-cm-diam., 7.5-cm-long tungsten target. Charged particles are removed from the well-collimated neutron beam by permanent magnets. Since the duration of the beam pulse ("micropulse") from the LAMPF accelerator is short, approximately 300 ps, neutron energies can be determined by time-of-flight (TOF) techniques. The flight path used for this experiment was oriented at 15° with respect to the incident proton beam. The distance between the neutron production target and the ^{40}Ca sample was 18.7 m.

The sample consisted of a cylindrical piece of natural calcium metal 6.4 cm in diameter and 7.6 cm long. The sample was oriented with its symmetry axis perpendicular to the reaction plane and was completely contained within the cross section of the neutron beam. The beam profile was determined by measuring the count rate in a small plastic scintillator as it was moved vertically and horizontally across the beam spot.

During the experiment the neutron flux was measured continuously by a fission chamber [22] through which the beam passes. This device consists of a 0.01-mm-thick stainless-steel foil coated with ^{238}U and mounted in an ion chamber. Neutrons passing through the chamber induce fission reactions that are detected through the ionization of the chamber gas by the recoiling fission fragments. Because the fission fragments deposit large amounts of energy in the chamber, fission events are well resolved from background alpha-particle-decay events. Figure 1 is a plot of the neutron flux per proton micropulse per solid angle per MeV of neutron energy for the 15° flight path. In typical WNR operation there are 17 000 micropulses per second.

The γ-ray spectrometer used for this experiment is illustrated in Fig. 2. It consists of a 10.2-cm-diam by 15.2-cm-long bismuth germanate (BGO) crystal coupled to a 12.7-cm-diam Hamamatsu R1250 photomultiplier tube. The anode signal is used for timing and a dynode signal provides the γ-ray pulse height. The BGO crystal sits inside a plastic scintillator (Bicron Corp. BC-400) anticoincidence shield that is used to veto cosmic rays and events in which radiation escapes from the BGO crystal. The shield is 5.1 cm thick in front and 6.7 cm thick along the sides of the BGO crystal and is viewed by six 5.1-cm-diam Burle 8575 photomultiplier tubes. All photomultiplier tube bases used in the spectrometer were designed for high count-rate stability.

With the exception of the tungsten aperture, the entire detector is surrounded with 10.2 cm of lead and 20.3 cm of polyethylene and borated polyethylene shielding. To reduce the flux of neutrons scattered from the sample into the detector, the tungsten aperture was blocked by 22.9 cm of ^{6}LiD. With this system, we were able to reject

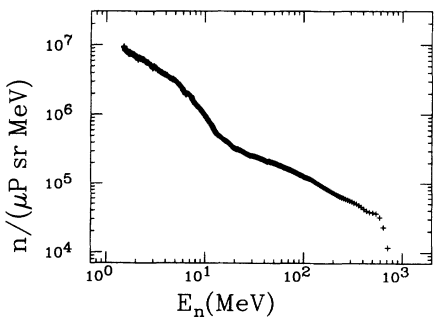

FIG. 1. Neutron flux from the WNR spallation neutron source measured at 15°.

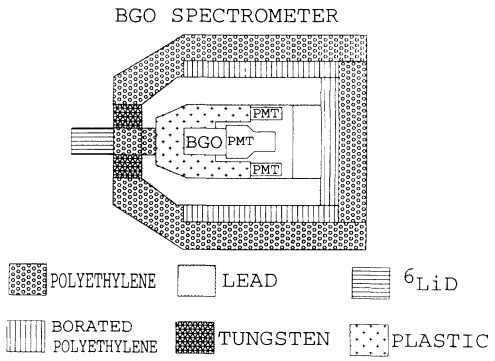

FIG. 2. Schematic diagram of the BGO spectrometer used in this experiment.

approximately 98.5% of the cosmic rays that survive the passive shielding.

Figure 3 shows the response of the detector system to gamma rays from the reaction $^{12}C(n,x\gamma)$ for incident neutron energies ranging from 17 to 28 MeV. The gamma ray was detected at 135°. The peak at channel 125 is from decays of the $J^\pi=1^+$, $E_x=15.11$ MeV level of ^{12}C. The full width at half maximum (FWHM) of the peak is 7.7%. We calculate Doppler broadening at $E_n=30$ MeV for $^{12}C(n,n'\gamma)$ to be less than 2.7%.

The neutron energy was determined by starting a time-to-amplitude converter (TAC) with the detector signal and stopping it with a delayed signal generated by the passage of a proton pulse from the LAMPF accelerator through a time pickoff unit. Pileup events were rejected by standard techniques [23]. Computer deadtime was minimized by using buffered analog-to-digital converters (ADC) (LeCroy model 3512) which were read out during the 16 ms between macropulses. A fixed electronic deadtime of 10 μs followed each trigger during which the ADC's were gated off and no events were accepted. Losses due to pileup as well as electronic deadtime were corrected for by scaling the number of times a valid trigger was generated and comparing it to the total number of events actually recorded. Total corrections for all losses were 9.5% and 9.4% at the fore and aft angles, respectively.

Measurements were made at 55°, 90°, and 125° with respect to the neutron beam direction. The total beam time at each setting was roughly 160, 90, and 220 h, respectively. Corresponding center-of-mass angles over the neutron energy range from 8 to 44 MeV for the forward setting ranged from 54.7° to 54.9° and from 125.2° to 125.4° for the aft setting. Systematic uncertainties in detector angles were estimated to be about 0.3°. To minimize systematic errors in measuring the asymmetries, runs at 55° were interspersed with ones at 125°, and neutron flux was adjusted by changing the collimation between forward and back angle runs to yield approximately equal count rates in the detector.

Prior to this experiment, as a test of our setup, we measured the γ-ray angular distribution from decay of the 15.11 MeV, $J^\pi=1^+$ level in ^{12}C produced by the $(n,n'\gamma)$ reaction. No significant asymmetries were observed.

III. ANALYSIS AND RESULTS

During the experiment the data were recorded event by event for later analysis. Each event consisted of four parameters: BGO pulse height, plastic pulse height, neutron TOF, and a BGO-plastic timing parameter. The data were examined and corrected in approximately 4 h intervals of run time for gain shifts in the BGO pulse height and time shifts in the neutron TOF spectra.

After eliminating events that are in coincidence with the plastic shield one is left with a two-parameter spectrum of counts versus γ-ray pulse height and neutron TOF. Figure 4 is a projection of the 55° two-parameter spectrum onto the TOF axis. Since timing is started by a spectrometer discriminator signal and stopped by a delayed signal from a time pickoff unit triggered by the primary proton beam, the right side of the spectrum corresponds to short times of flight, or high neutron energies. Although the number of events per unit energy decreases with increasing neutron energy, because of the nonlinear relation between neutron energy and flight time, dE_n/dt is time dependent and the number of events per unit time increases at shorter times of flight. An unfavorable consequence of this energy compression is that at short times of flight the neutron energy resolution of the system worsens. However, an offsetting advantage when measuring a rate that falls with increasing energy is that, since the cosmic-ray background is constant across the TOF spectrum, the number of cosmic rays per neutron energy bin decreases with increasing energy. The peak to the right of the neutron induced events corresponds to events induced by photons coming from the neutron production

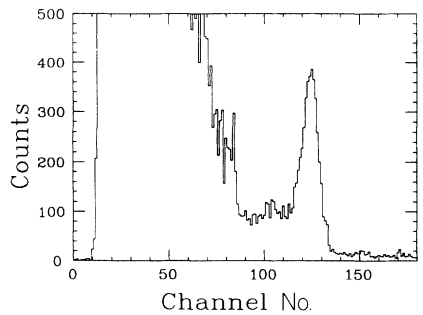

FIG. 3. Detector response to photons from the $^{12}C(n,x\gamma)$ reaction for $17 \leq E_n \leq 28$ MeV.

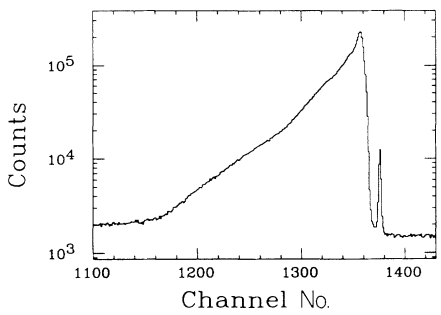

FIG. 4. Time-of-flight spectrum measured at 55° for the $^{40}Ca+n$ reaction.

target. This "gamma flash" is useful because, with a knowledge of the flight path length, it provides a reference time that is used to calculate neutron energies and avoids the need for knowledge of the exact timing of the signals from the beam pickoff unit and the spectrometer.

A relative time scale for the TOF spectrum was established from a polynomial fit to a spectrum generated with a time calibrator (ORTEC 462). Although a quadratic fit was used, the differences between using a quadratic and a linear polynomial amounted to less than 0.1 MeV at 8 MeV and less than 0.5 MeV at 44 MeV. We produced a γ-ray energy calibration by making pulse-height projections for various neutron energy bins over the GDR and observing the locations of the capture γ-ray peak. The highest gamma energy at which we could reliably observe a peak was 27.9 MeV. We found the conversion from channel number to energy in the region of the GDR to be linear and assumed that it was linear at higher energies.

From the two-parameter spectrum of γ-ray pulse height versus neutron TOF, we generated a background pulse-height spectrum by summing over a portion of the TOF channels to the right of the gamma flash. These events are time-random background, presumably from cosmic rays and time-correlated events induced by low-energy neutrons from a previous beam burst. The gamma pulse heights of the events induced by low-energy neutrons are too low to be of concern in this experiment. The "random" γ-ray spectrum so generated was appropriately normalized and subtracted from each projected pulse-height spectrum.

To correct for beam-correlated background, the counts in a window just above the ground-state capture window were subtracted from the counts in the capture window. This background consists of several components including capture processes with high Q values—notably neutron capture on atmospheric nitrogen. Other contributions include background from the primary beam transport system and from other experiments running in the vicinity as well as unrejected pileup. Although this correction was generally small, for the forward angle at 42 MeV, it was about 60%. The background correction decreased to 30% at 32 MeV and continued to decrease below that. The effect of the correction on the measured asymmetry was small with the main effect being to increase the error bars.

The procedure used to extract the capture yield struck a balance between the desire to minimize contamination of the ground-state yield by capture to the first excited state of ^{41}Ca ($E_x = 1.943$ MeV) with the need for a reasonable level of statistics. Because the capture gamma-ray energy is a function of the neutron energy, the effective capture gamma energy resolution depends on the neutron energy resolution. The 2.2-ns time resolution of the detector system corresponds to a neutron energy resolution of about 1.0 MeV at $E_n = 44$ MeV. The response of the detector system to a monoenergetic gamma of high energy is not well characterized; however, since the response of the detector to a 15.11-MeV gamma ray is similar to that reported by Wagenaar and coworkers [24] for a similar system, we extrapolate their resolution results, which were based on upper half width at half maximum measurements, to estimate a resolution of about 1.6 MeV at the highest gamma energies in this work.

Capture yields for each TOF channel were obtained by summing the pulse-height spectrum over an energy window around the ground-state capture γ ray. Because of the worsening neutron energy resolution as a function of neutron energy, the width of the window depended on energy and ranged from 1.7 MeV at $E_n = 8$ MeV to 0.88 MeV at $E_n = 44$ MeV. Figure 5 shows the gamma pulse-height spectrum for a single TOF channel from the 125° data at a neutron energy of 10.3 MeV which is at the peak of the GDR. At this energy the width of the TOF channel is 50 keV. The gamma window shown is 1.7 MeV wide. This figure was produced from raw data without subtracting any background.

The capture yields extracted by the above procedure were then binned in neutron energy in 1 MeV steps from 8 to 20 MeV and in 4 MeV steps from 20 to 44 MeV. To form the asymmetry plot shown in Fig. 6(a), the yields at each angle and energy were normalized by the corresponding neutron fluence measured by the fission chamber. Additionally we have applied a constant relative normalization between the forward and backward angle which arises mainly from the difference of the beam profile on target between the two neutron beam collimation settings. There are also small contributions to the normalization due to the difference in the amount of gamma and neutron attenuation and multiple scattering by the sample between the two angles as well as from the difference in center-of-mass solid angles. Both of these small contributions are nearly energy independent.

The relative normalization was empirically estimated to be 0.75 by forcing the asymmetries between $E_n = 8$ and 13 MeV to agree with previous measurements [25]. A subsequent calculation, in which the effect of the collimation on the beam profile was modeled by Monte Carlo techniques, yielded a value for the relative normalization of 0.78.

Figure 6(b) shows the asymmetry generated by the same procedure except that a constant width gamma-ray energy window of 1.7 MeV was used. Here we have better statistics but, at the highest neutron energies, expect more contamination from capture to excited states. There do not appear to be significant differences between the two analyses. Both parts of Fig. 6 also show the results of other authors for comparison.

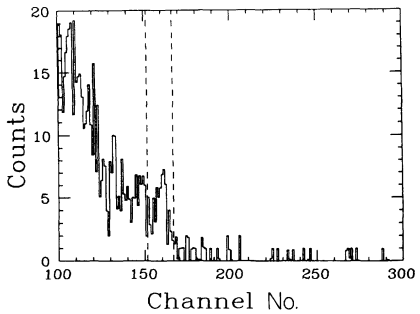

FIG. 5. γ-pulse-height spectrum for a 50-keV neutron-energy bin for $E_n = 10.3$ MeV and $\theta = 125°$.

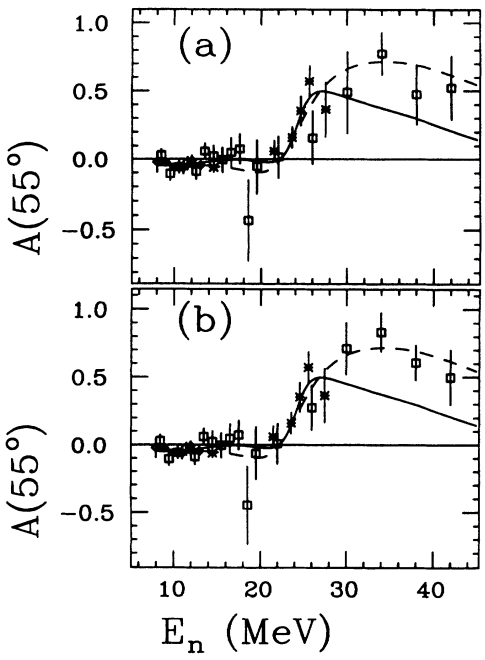

FIG. 6. Plot of $A(55°)$. Parts (a) and (b) represent different analysis techniques (see text). Previous data are represented by diamonds [25] and stars [11] and the present data by squares. The solid curve is from the DSD calculation and the dashed curve is from the calculation in which the PRM was used to calculate the $E1$ amplitude.

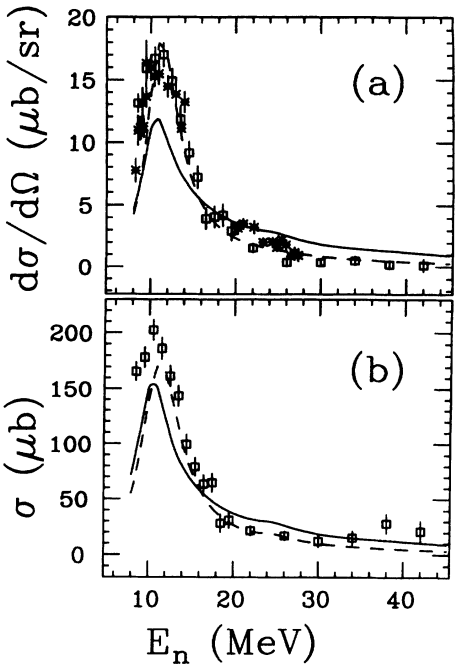

FIG. 7. (a) Plot of the 90° differential cross section showing previous work as stars [11] and the present work as squares, and (b) plot of the total cross section. The solid curve is from the DSD calculation and the dashed curve is from the calculation in which the PRM was used to calculate the $E1$ amplitude.

Figure 7 illustrates the cross sections from this experiment. Part (a) is the 90° differential cross section and part (b) is the quantity

$$2\pi\left[\frac{d\sigma(55°)}{d\Omega}+\frac{d\sigma(125°)}{d\Omega}\right]$$

which is approximately equal to the total cross section under the assumption that quadrupole and higher-order amplitudes are much smaller than the dipole amplitude. This can be seen by considering an expansion of the angular distribution in terms of Legendre polynomials and noting that odd terms disappear in the above expression and that $P_2=0$ at the measured angles. The procedure used to produce this figure is basically the same as that for generating Fig. 6(b) except that the energy dependence of the attenuation of neutrons and photons by the sample was included. To establish a cross-section scale, detector efficiencies as a function of γ-ray energy were calculated using the Monte Carlo program CYLTRAN [26], modified to track coincidences between the BGO and plastic shield. There is an uncertainty of 20% in the overall normalization of Fig. 7 for energies below about 20 MeV. The main contributions to this are the uncertainty in the thickness of the ^{238}U deposit in the fission chamber and uncertainties in the detector efficiency calculation. Above 20 MeV, uncertainties in the normalization may be much larger. Additionally the relative size of the beam correlated background grows with energy. This is especially true in the case of the 90° cross section where the data were taken with poorer quality beam than in the case of the other two angles.

IV. DISCUSSION AND CONCLUSIONS

In the cross section plots for the ^{40}Ca(n,γ_0) reaction shown in Fig. 7, as well as in the asymmetry plots in Fig. 6, the energy coordinate of each point represents the center of the bin. Also shown in Fig. 7(a) are the results of Berqvist *et al.* [11] with which the present data are in agreement. The asymmetries deduced in this work and shown in Fig. 6 also are in agreement with the data of Berqvist *et al.* [11] and Wender *et al.* [25]. A notable feature of the present data is the large asymmetries found at high energies.

Some recent (γ,n) measurements [13–15] on ^{40}Ca, ^{nat}Pb, and ^{nat}Cd, in which final states were not resolved, systematically found asymmetries rising to large values similar to those observed here.

Most of the presently available nucleon capture and photonuclear data are consistent with an $E2$ resonance interfering with an $E1$ background. It has been productive to describe these results in terms of the DSD model [27,28]. Berqvist *et al.* [11] performed a DSD calculation for the ^{40}Ca(n,γ_0) reaction and found that they could not reproduce the cross section in the vicinity of the GDR without including a second resonance. They assumed this resonance was the isospin forbidden $T_>$ component of the GDR. The solid lines shown in Figs. 6 and 7 were generated with the parameters reported by Berqvist *et al.* [11] except that the second GDR ($T_>$) component has been omitted. The asymmetry shown by the solid line in Fig. 6 is insensitive to the presence of the second GDR component and falls well below the data at high energies.

We have investigated what changes in the parameters

of the DSD calculation would be required to obtain agreement with our measured asymmetries at high energy. For both the dipole ($L=1$) and quadrupole ($L=2$) isovector resonances the calculation used a complex particle-vibration coupling [29,30] of the form

$$h_L \propto r^L S_L \left[V_1 f_r(r) - iW_1 4b \frac{df_i(r)}{dr} \right],$$

where $f_r(r)$ and $f_i(r)$ are the real and imaginary Wood-Saxon form factors, b is the diffuseness parameter, and V_1 and W_1 are the isovector potential depths. The same values of V_1 and W_1 were used for both the dipole and quadrupole form factors. S_L is the fraction of the classical sum rule assumed for each resonance. The optical model parameters used are based on those of Ref. [31]. Other details of the calculation including the parametrization of the complex isoscalar form factor can be found in Ref. [11]. The present data coupled with those of Ref. [11] suggest the need for both a larger width (Γ_Q) and a larger value of the ratio (R) of the magnitude of the resonating amplitude, assumed to be quadrupole, to that of the background dipole amplitude. From the data we infer the need for a value of $\Gamma_Q > 8$ MeV (see the appendix of Ref. [11]) and a value of R of at least 3 times that of Ref. [11] to be appropriate.

Assuming conservation of isospin, one can excite only the $T_<$ component of an isovector resonance through the capture of a $T=\frac{1}{2}$, $T_Z=\frac{1}{2}$ neutron on a nucleus with $T_Z \geq 0$. The expected [11] ratio of excitation strengths for the two isospin components of the IVGQR is

$$\frac{S_>}{S_<} = \frac{1}{T_0} \frac{1-2T_0/A}{1+2/A} = 1.9 \quad \text{for } {}^{41}\text{Ca} .$$

In the calculation of Berqvist *et al.* [11] it was assumed that 35% of the classical $E2$ sum rule strength was present in the IVGQR which is the maximum expected for the $T_<$ component. Therefore increasing the IVGQR strength by a factor of three seems unreasonable.

We have found that we are able to achieve a reasonable fit to the asymmetry data by including a $T_> E2$ resonance slightly above the location of the $T_<$ IVGQR component at 20% of the expected maximum $T_>$ strength. This is the same fraction of the expected maximum strength that Berqvist *et al.* [11] used when they added a $T_>$ GDR component to fit the cross section data. Including the $T_>$ resonance implies significant isospin violation for which there is little theoretical or experimental justification.

Figure 7 sheds light on the nature of the possible problem with the DSD calculation. In addition to the discrepancies noted by Berqvist *et al.* [11] just above the peak of the GDR which prompted them to add the isospin violating $T_>$ component of the GDR to the calculation, the present work suggests that the calculation overpredicts the cross section over much of the region above the GDR starting at about 20 MeV. This observation is tentative because of the uncertainties in the normalizations of the high-energy points. The underprediction of the maximum asymmetry may be a result of the overprediction of the $E1$ amplitude by the DSD calculation because the maximum value to which the asymmetry rises depends on the ratio of the magnitudes of the two interfering amplitudes as well as the phase difference between them.

In Fig. 8 we illustrate the cross sections that would arise from some of the individual amplitudes in the calculation. Above the peak of the GDR the calculation is dominated by the direct $E1$ contribution. There is little freedom in the DSD model to adjust the direct capture amplitude. However, Dietrich [32] pointed out that in an exact formulation of the DSD model the resonating amplitude must have a component that approximately cancels the direct amplitude. This may fail to occur because of the lack of a uniform treatment of the two amplitudes.

The pure resonance model (PRM) of nucleon capture [32,33] is formally equivalent to the DSD model but contains no direct amplitude and therefore does not depend on the near cancellation of two separate components. The PRM was introduced to reduce sensitivities to the parametrization of the physically ambiguous, imaginary part of the form factor.

The results of a calculation in which the $E1$ amplitude was treated in the framework of the PRM (Ref. [33] version) is illustrated by the dashed lines in Figs. 6 and 7. This version of the PRM is an approximation to the exact version of Ref. [32]. In the approximation, a small but difficult to calculate resonating term is neglected. This corresponds to neglecting $E1$ strength not coupled to the GDR. The $E2$ amplitudes were calculated in the DSD framework. The form factors used are the same as those in the original calculation except that no imaginary $E1$ component was used and the strengths of the isovector potentials V_1 and W_1 (for the IVGQR) were increased by 40% to 168 and 56 MeV, respectively. We have also adjusted the resonance parameters. In the new calculation the GDR energy and width have been set to 19.0 and 4.6 MeV and the IVGQR energy and width to 31 and 10 MeV, respectively. The calculation does not include compound nuclear components which contribute at energies below the peak of the GDR.

The PRM calculation does a better job of fitting the observed cross section and asymmetry than does the DSD calculation. In this case, the formulation of the PRM in which there is no explicit direct amplitude is apparently an advantage in fitting the data above the GDR.

A word of caution concerning the interpretation of

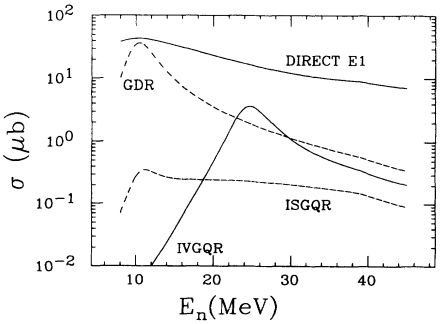

FIG. 8. Plot of the total cross sections that arise from the major individual components in the DSD calculation of Ref. [11].

these calculations is in order. We assumed that the interfering amplitudes producing the asymmetry are $E1$ and $E2$ and that no others are present. Since interference measurements are very sensitive and since the amplitudes in the region of the IVGQR are small, the asymmetry can be strongly influenced by amplitudes which we have not considered. The rise in the cross section observed in the last two points of Fig. 7, if real, could indicate the presence of such amplitudes. Since this capture experiment involved a single photon in the exit channel, it is, unlike charge exchange experiments, insensitive to monopole amplitudes. Based on an asymmetry measurement, little else can be determined about the multipolarity of the contributing amplitudes in a model independent way.

V. SUMMARY

The present experiment is an illustration of the usefulness of a spallation neutron source in the study of the energy dependence of a low intensity nuclear process such as radiative capture. The experiment supports the previous observation in nucleon capture and photonuclear reactions of an energy dependent fore-aft asymmetry in the gamma-ray angular distribution. This asymmetry has been interpreted in terms of interference between a resonant $E2$ amplitude (IVGQR) and direct and resonant $E1$ amplitudes by means of the DSD model. The present data are in good agreement with previous data sets in the region where they overlap. In the higher-energy region, where no other data exists, the measured asymmetries are larger than predicted by DSD calculations. The cross section data suggest that this discrepancy may be because of an overprediction of the direct $E1$ amplitude. A calculation using the PRM [33] for the GDR yields better fits to the cross section and asymmetry data.

Further experiments of this type probing other nuclei as well as spectroscopically complete experiments in more favorable spin systems would be useful in advancing our understanding of the IVGQR. More sophisticated calculations would also be welcome.

[1] A. van der Woude, Prog. Part. Nucl. Phys. (G.B.) **18**, 217 (1987).

[2] Josef Speth and Adriaan van der Woude, Rep. Prog. Phys. **44**, 719 (1981).

[3] *Electric and Magnetic Giant Resonances in Nuclei-International Review of Nuclear Physics* —Vol. 7, edited by J. Speth (World Scientific, Singapore, 1991).

[4] K. A. Snover, J. Phys. C **4**, 337 (1984).

[5] Rainer Pitthan, in *Giant Multipole Resonances—Proceedings of the Giant Resonance Topical Conference, Oak Ridge, 1979,* edited by Fred F. Bertrand (Harwood, New York, 1980).

[6] R. J. Stewart, R. C. Morrison, and D. E. Frederick, Phys. Rev. Lett. **23**, 323 (1969).

[7] K. A. Snover, K. Ebisawa, D. R. Brown, and P. Paul, Phys. Rev. Lett. **32**, 317 (1974).

[8] G. Feldman, L. H. Kramer, H. R. Weller, E. Hayward, and W. R. Dodge, Phys. Rev. C **43**, 223 (1991).

[9] J. M. Eisenberg and W. Greiner, *Nuclear Theory Vol. 2—Excitation Mechanisms of the Nucleus, Third Revised Edition* (North-Holland, Amsterdam, 1988).

[10] D. M. Drake, S. Joly, L. Nilsson, S. A. Wender, K. Aniol, I. Halpern, and D. Storm, Phys. Rev. Lett. **47**, 1581 (1981).

[11] I. Bergqvist, R. Zorro, A. Håkansson, A. Lindholm, L. Nilsson, N. Olsson, and A. Likar, Nucl. Phys. A **419**, 509 (1984).

[12] T. W. Phillips and R. G. Johnson, Phys. Rev. C **20**, 1689 (1979).

[13] T. Murakami, I. Halpern, D. W. Storm, P. T. Debevec, L. J. Morford, S. A. Wender, and D. H. Dowell, Phys. Rev. C **35**, 479 (1987).

[14] D. W. Storm, I. Halpern, C. A. Gossett, T. Murakami, D. P. Rosenzweig, D. R. Tieger, P. T. Debevec, A. Freytag, L. J. Morford, S. A. Wender, and D. H. Dowell, Can. J. Phys. **65**, 677 (1987).

[15] T. Murakami, C. A. Gossett, I. Halpern, D. P. Rosenzweig, D. W. Storm, D. R. Tieger, P. T. Debevec, A. Freytag, L. J. Morford, S. A. Wender, and D. H. Dowell, J. Phys. G **14**, S275 (1988).

[16] A. Erell, J. Alster, J. Lichtenstadt, M. A. Moinester, J. D. Bowman, M. D. Cooper, F. Irom, H. S. Matis, E. Piastzky, and U. Sennhauser, Phys. Rev. C **34**, 1822 (1986).

[17] F. Irom, J. D. Bowman, G. O. Bolme, E. Piasetzky, U. Sennhauser, J. Alster, J. Lichtenstadt, M. Moinester, J. N. Knudson, S. R. Rokni, and E. R. Siciliano, Phys. Rev. C **34**, 2231 (1986).

[18] N. Auerbach and Amir Klein, Phys. Rev. C **28**, 2075 (1983).

[19] S. L. Tabor, G. Neushaefer, J. A. Carr, F. Petrovich, C. C. Chang, A. Guterman, M. T. Collins, D. L. Friesel, C. Glover, S. Y. van der Werf, and S. Raman, Nucl. Phys. A **422**, 12 (1984).

[20] P. W. Lisowski, C. D. Bowman, G. J. Russell, and S. A. Wender, Nucl. Sci. Eng. **106**, 208 (1990).

[21] S. A. Wender and G. F. Auchampaugh, in *Capture Gamma-Ray Spectroscopy and Related Topics—1984, Proceedings of the International Symposium,* Knoxville, Tennessee, edited by S. Raman (AIP, New York, 1985).

[22] S. A. Wender, R. C. Haight, R. O. Nelson, C. M. Laymon, A. Brown, S. Balestrini, W. McCorkle, T. Lee, and N. W. Hill, Los Alamos National Laboratory Report No. LA-UR-90-3399, 1990 (unpublished).

[23] S. L. Blatt, J. Mahieux, and D. Kohler, Nucl. Instrum. Methods **60**, 221 (1968).

[24] Douglas J. Wagenaar, N. R. Roberson, and H. R. Weller, Nucl. Instrum. Methods A **234**, 109 (1985).

[25] S. A. Wender, N. R. Roberson, M. Potakar, H. R. Weller, and D. R. Tilley, Phys. Rev. Lett. **41**, 1217 (1978).

[26] J. A. Halbleib, Sr. and W. H. Vandevender, Sandia Laboratories Report No. SAND-74-0030, 1974 (unpublished).

[27] C. F. Clement, A. M. Lane, and J. R. Rook, Nucl. Phys. **66**, 273 (1965).

[28] G. E. Brown, Nucl. Phys. **57**, 339 (1964).

[29] M. Potakar, Phys. Lett. **46B**, 346 (1973).

[30] G. E. Satchler, Nucl. Phys. A **195**, 1 (1972).

[31] W. Tornow *et al.*, Nucl. Phys. A **385**, 373 (1982).

[32] F. S. Dietrich, in [21].

[33] F. S. Dietrich and A. K. Kerman, Phys. Rev. Lett. **43**, 114 (1979).

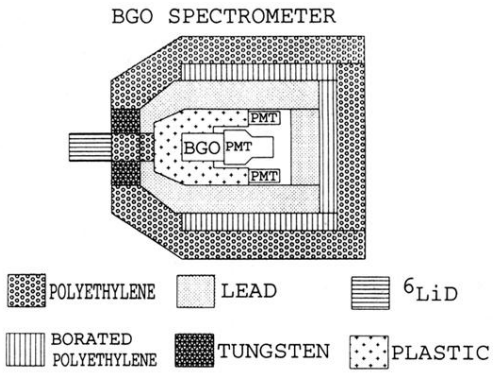

FIG. 2. Schematic diagram of the BGO spectrometer used in this experiment.